

Boundary Localized Terms in Universal Extra-Dimensional Models through a Dark Matter perspective

Anindya Datta^{1*}, Ujjal Kumar Dey^{1,2†}, Amitava Raychaudhuri^{1‡}, Avirup Shaw^{1§}

¹⁾ *Department of Physics, University of Calcutta, 92 Acharya Prafulla Chandra Road, Kolkata 700009, India*

²⁾ *Harish-Chandra Research Institute, Chhatnag Road, Jhansi, Allahabad 211019, India*

Abstract

In universal extra dimension (UED) models with one compactified extra dimension, a \mathbf{Z}_2 symmetry, termed KK-parity, ensures the stability of the lightest Kaluza-Klein particle (LKP) which could be a viable dark matter candidate. This symmetry leads to two fixed points. In non-minimal versions of UED boundary-localized (kinetic or mass) terms (BLT) for different fields are included at these fixed points and KK-parity may be violated. However, BLTs with same strength at both points induce a new \mathbf{Z}_2 symmetry which restores the stability of the LKP. We show that the BLTs serve to relax the bounds set on the compactification scale in UED by the observed dark matter relic density. At the same time, the precision of the dark matter measurements severely correlates the BLT parameters of gauge bosons and fermions. Depending on the parameter values, the LKP can be chosen to be the level-1 photon, which is essentially the $B^{(1)}$, or the level-1 Z -boson, basically the $W_3^{(1)}$. We find that in the latter case the relic density is too small if the $W_3^{(1)}$ has a mass ~ 1 TeV. We also explore the prospects of direct detection of an LKP which matches the observed dark matter relic density.

PACS Nos: 11.10.Kk, 14.80.Rt, 95.35.+d

Key Words: Universal Extra Dimension, Kaluza-Klein, Dark Matter

I Introduction

With the rapid advancement in observational techniques cosmological parameters have been measured with unprecedented precision. In step, the evidence of a dark matter (DM) component in the universe has been steadily strengthened. The Planck Satellite Mission [1] reveals that the directly observable baryon density of the universe is only about 4.9%, whereas dark matter constitutes about 26.8% of the total energy of the universe, the rest is due to dark energy. This partitioning is along the lines indicated earlier by the Wilkinson Microwave Anisotropy Probe [2] and other observations.

Recently, on the basis of measurements made at the International Space Station, the AMS-02 collaboration [3] has published striking indications for an excess of the positron to electron ratio which could

*email: adphys@caluniv.ac.in

†email: ujjaldey@hri.res.in

‡email: palitprof@gmail.com

§email: avirup.cu@gmail.com

be an indirect evidence for dark matter. This further sharpens similar observations from PAMELA [4] and Fermi-LAT [5].

On the particle physics side the standard model (SM) is a major success in explaining physics up to the TeV scale and has been repeatedly tested at collider experiments. Very recently the discovery of a Higgs particle [6, 7] has put the SM on a stronger footing. Yet the model leaves a few pertinent questions unanswered, e.g., existence of neutrino masses, matter-antimatter asymmetry, the hierarchy problem, etc. Moreover, the Standard Model does not solve the DM conundrum as there is no suitable candidate that can fulfill the requirement. Although initially neutrinos or axions were hoped to be the required DM particle, from present day cosmological observations they are disfavoured.

The requirement of a dark matter candidate has been one of the important motivations to go beyond SM. Supersymmetry (SUSY) is by far the most popular and thus extensively studied beyond-standard-model scenario. The imposition of a discrete symmetry – R-parity – ensures the stability of the lightest supersymmetric particle (LSP) which can be a competent DM candidate. Alternative variants within the SUSY framework predict different LSPs. For a review of dark matter in the supersymmetric context see, for example, [8]. A number of DM candidates have also been put forward in non-supersymmetric scenarios. In Little Higgs Models, for example, a conserved discrete symmetry, known as T-parity, assures the stability of the lightest T-odd particle, which is typically a heavy photon [9] and it can be a dark matter candidate. A common theme is that in any model attempting to address the dark matter question, there is some \mathbf{Z}_2 symmetry that makes the lightest symmetry-odd particle stable and, needless to say, that particle should also satisfy the cosmological observational data, such as relic density.

Extra-dimensional models, an alternate extension of the SM, also predict their own dark matter candidate. In this work we study a model [10] where all the SM fields can propagate in the bulk. We consider models with one extra spacelike flat compactified dimension, y . If R is the radius of compactification, this coordinate can be considered to run from 0 to $2\pi R$. All particles – scalars, spin-1/2 fermions, and gauge bosons – are represented by five-dimensional fields. These are often conveniently expressed in terms of towers of four-dimensional Kaluza-Klein (KK) states.

In the simplest model the zero-modes of the KK-towers are the SM particles. The KK states of all particles at the n -th level have the same mass, n/R . In addition, a \mathbf{Z}_2 symmetry ($y \leftrightarrow -y$) needs to be imposed to ensure the observed chirality of zero-mode fermions. The extra dimension is compactified, in this manner, on an orbifold S^1/Z_2 . The $y \leftrightarrow -y$ symmetry leads to a conserved KK-parity $= (-1)^n$, where n is the KK-level. The SM particles ($n = 0$) are of even parity while the KK-states of the first level are odd. The conservation of KK-parity ensures that the lightest $n = 1$ particle cannot decay to SM particles and hence is a potential dark matter candidate, the Lightest Kaluza-Klein Particle (LKP). This constitutes what is known as the Universal Extra Dimension (UED) Model.

The S^1/Z_2 orbifold compactification results in fixed points at $y = 0$ and $y = \pi R$. At these two points one can allow four-dimensional kinetic and mass terms for the KK-states. In fact, these terms are also required as counterterms for cut-off dependent loop-induced contributions [11] of the five-dimensional theory. In the minimal Universal Extra-Dimensional Models (mUED) [12, 13] these terms are fixed by requiring that the five-dimensional loop contributions are exactly compensated at the cutoff scale Λ and the boundary values of the corrections, e.g., logarithmic mass corrections of KK particles, can be taken to be zero at the scale Λ . These loop contributions can remove the mass degeneracy among states at the same KK-level n .

The viability of the LKP – a weakly interacting massive particle (WIMP) – as a dark matter candidate satisfying the cosmological relic density constraint has been examined earlier [14, 15, 16]. These studies within the context of UED or mUED at various levels of sophistication [17, 18] – e.g., inclusion of channels of scattering and coannihilation – indicate that the $n = 1$ excitation of the hypercharge gauge boson B could be a possible candidate for the dark matter of the universe.

In this work we allow boundary terms to be unrestricted by the special choice in mUED. In this sense the model can be termed non-minimal UED (nmUED). However, we do maintain the boundary terms to be equal at both fixed points. This will preserve a discrete \mathbf{Z}_2 symmetry which exchanges $y \longleftrightarrow (y - \pi R)$ and makes the LKP stable.

The compactification radius R and the cut-off Λ are the two basic parameters of these extra-dimensional models and there have been several explorations of constraints on them in UED and its variants. It has been shown that in these models to one-loop order electroweak observables receive finite corrections [19]. Thus it is not unreasonable to compare the predictions of the theory with experimental data to set bounds on R and Λ . For example, from muon $(g - 2)$ [20], flavour changing neutral currents [21, 22, 23], $Z \rightarrow b\bar{b}$ decay [24], the ρ parameter [10, 25], and other electroweak precision tests [26, 27], it is found that $R^{-1} \gtrsim 300 - 600$ GeV. The possibility of a not too high R^{-1} motivates the continuing search for signatures of the model at the Tevatron and the LHC [28, 29] and also at the ILC or CLIC [30] in the future.

Here we use the dark matter relic density constraint to place limits on R^{-1} taking the LKP as the DM candidate. We consider the impact of the boundary-localized kinetic terms (BLKT) on the masses of the KK states and, to our knowledge for the first time¹, also on the KK couplings. In the process the masses of the KK excitations deviate from their UED value of n/R and the couplings of these particles exhibit a departure from the standard model values. We show that together this makes additional room for the possible values of the compactification radius beyond what is permitted in UED.

In the next section, we briefly review the nmUED scenario with boundary-localized kinetic terms. To set up the notation this is followed by a recapitulation of the steps in the estimation of dark matter relic density. We come next to our results where we identify the regions of parameter space already excluded by the current limits on the relic density. In the following section we consider the possibility of direct detection of the nmUED dark matter candidate for the range of parameters consistent with the relic density bound. We end with our summary and conclusions. Non-trivial nmUED vertices used in this work are collected together in an Appendix.

II Non-minimal UED

In nmUED one considers kinetic and mass terms localized at the fixed points. Here we restrict ourselves to boundary-localized kinetic terms only [32] - [38].

Specifically we consider a five-dimensional theory with additional kinetic terms localized at the boundaries at $y = 0$ and $y = \pi R$. For example, for free fermion fields $\Psi_{L,R}$ whose zero-modes are the chiral

¹While this paper was being written up another paper [31] has appeared where the modification of the couplings due to five-dimensional wave-functions is considered in the context of fermion bulk mass terms along with BLKT.

projections of the SM fermions the five-dimensional action with BLKT is [39]:

$$S = \int d^4x dy \left[\bar{\Psi}_L i\Gamma^M \partial_M \Psi_L + r_f \{ \delta(y) + \delta(y - \pi R) \} \phi_L^\dagger i\bar{\sigma}^\mu \partial_\mu \phi_L + \bar{\Psi}_R i\Gamma^M \partial_M \Psi_R + r_f \{ \delta(y) + \delta(y - \pi R) \} \chi_R^\dagger i\sigma^\mu \partial_\mu \chi_R \right], \quad (1)$$

with $\sigma^\mu \equiv (I, \vec{\sigma})$ and $\bar{\sigma}^\mu \equiv (I, -\vec{\sigma})$, $\vec{\sigma}$ being the (2×2) Pauli matrices. Here r_f parametrizes the strength of the boundary terms which, for illustrative purposes, we choose to be the same for Ψ_L and Ψ_R in this section.

It is convenient to express the five-dimensional fermion fields using two component chiral spinors² [39]:

$$\Psi_L(x, y) = \begin{pmatrix} \phi_L(x, y) \\ \chi_L(x, y) \end{pmatrix} = \sum_{n=0}^{\infty} \begin{pmatrix} \phi_n(x) f_L^{(n)}(y) \\ \chi_n(x) g_L^{(n)}(y) \end{pmatrix}, \quad (2)$$

$$\Psi_R(x, y) = \begin{pmatrix} \phi_R(x, y) \\ \chi_R(x, y) \end{pmatrix} = \sum_{n=0}^{\infty} \begin{pmatrix} \phi_n(x) f_R^{(n)}(y) \\ \chi_n(x) g_R^{(n)}(y) \end{pmatrix}. \quad (3)$$

Below we analyse the case of Ψ_L in detail. The formulae for Ψ_R will be similar and can be obtained by making appropriate changes.

Using eq. (2) and varying the action functional – eq. (1) – results in coupled equations for the y -dependent wave-functions, $f_L^{(n)}, g_L^{(n)}$. Following standard steps³ one finds:

$$[1 + r_f \{ \delta(y) + \delta(y - \pi R) \}] m_n f_L^{(n)} - \partial_y g_L^{(n)} = 0, \quad m_n g_L^{(n)} + \partial_y f_L^{(n)} = 0, \quad (n = 0, 1, 2, \dots). \quad (4)$$

Eliminating $g_L^{(n)}$ one obtains the equation:

$$\partial_y^2 f_L^{(n)} + [1 + r_f \{ \delta(y) + \delta(y - \pi R) \}] m_n^2 f_L^{(n)} = 0. \quad (5)$$

Below we drop the subscript L on the wave-functions and denote them by f and g .

The boundary conditions which we impose are [33]:

$$f^{(n)}(y)|_{0^-} = f^{(n)}(y)|_{0^+}, \quad f^{(n)}(y)|_{\pi R^+} = f^{(n)}(y)|_{\pi R^-}, \quad (6)$$

$$\left. \frac{df^{(n)}}{dy} \right|_{0^+} - \left. \frac{df^{(n)}}{dy} \right|_{0^-} = -r_f m_n^2 f^{(n)}(y)|_{0}, \quad \left. \frac{df^{(n)}}{dy} \right|_{\pi R^+} - \left. \frac{df^{(n)}}{dy} \right|_{\pi R^-} = -r_f m_n^2 f^{(n)}(y)|_{\pi R}. \quad (7)$$

Under the above conditions one gets the solutions:

$$\begin{aligned} f^{(n)}(y) &= N_n \left[\cos(m_n y) - \frac{r_f m_n}{2} \sin(m_n y) \right], \quad 0 \leq y < \pi R, \\ f^{(n)}(y) &= N_n \left[\cos(m_n y) + \frac{r_f m_n}{2} \sin(m_n y) \right], \quad -\pi R \leq y < 0. \end{aligned} \quad (8)$$

where the masses m_n for $n = 0, 1, \dots$ arise from the transcendental equation:

$$(r_f^2 m_n^2 - 4) \tan(m_n \pi R) = 4r_f m_n. \quad (9)$$

²The Dirac gamma matrices are in the chiral representation with $\gamma_5 = \text{diag}(-I, I)$.

³More details in the same notations and conventions can be found in [38].

The solutions satisfy the *orthonormality* relations:

$$\int dy [1 + r_f \{\delta(y) + \delta(y - \pi R)\}] f^{(n)}(y) f^{(m)}(y) = \delta^{nm} . \quad (10)$$

The normalisation constant N_n is

$$N_n = \sqrt{\frac{2}{\pi R}} \left[\frac{1}{\sqrt{1 + \frac{r_f^2 m_n^2}{4} + \frac{r_f}{\pi R}}} \right]. \quad (11)$$

Note that the wavefunctions are combinations of a sine and a cosine function unlike in the case of mUED where it is one or the other of these trigonometric functions. This and the fact that the KK masses are solutions of eq. (9) rather than simply n/R are at the root of the novelty of nmUED over the other versions of the theory.

In our work we will deal only with the zero-modes and the $n = 1$ KK wave-functions of the five-dimensional fermion fields.

KK wave-functions for scalar and spin-1 fields exhibit very similar features as above. We illustrate this point through a five-dimensional gauge field, G_N ($N = 0 \dots 4$). The action with boundary kinetic terms can be similarly written as

$$S = -\frac{1}{4} \int d^4x dy [F_{MN} F^{MN} + r_G \{\delta(y) + \delta(y - \pi R)\} F_{\mu\nu} F^{\mu\nu}], \quad (12)$$

where $F_{MN} = (\partial_M G_N - \partial_N G_M)$ and r_G is the strength of the boundary term (equal at both fixed points) which is varied in our analysis⁴.

The expansion of the gauge field will be:

$$G_\mu(x, y) = \sum_{n=0}^{\infty} G_\mu^{(n)}(x) a^{(n)}(y), \quad G_4(x, y) = \sum_{n=0}^{\infty} G_4^{(n)}(x) b^{(n)}(y), \quad (13)$$

where the functions $a^{(n)}(y)$ and $b^{(n)}(y)$ are determined by the boundary conditions as discussed below. It is convenient to make the gauge choice: $G_4 = 0$.

Variation of the action yields the equations satisfied by the functions $a^{(n)}(y)$:

$$\partial_y^2 a^{(n)}(y) + [1 + r_G \{\delta(y) + \delta(y - \pi R)\}] m_n^2 a^{(n)}(y) = 0. \quad (14)$$

We use the boundary conditions

$$a^{(n)}(y)|_{0^-} = a^{(n)}(y)|_{0^+}, \quad a^{(n)}(y)|_{\pi R^+} = a^{(n)}(y)|_{\pi R^-}, \quad (15)$$

$$\left. \frac{da^{(n)}}{dy} \right|_{0^+} - \left. \frac{da^{(n)}}{dy} \right|_{0^-} = -r_G m_n^2 a^{(n)}(y)|_0, \quad \left. \frac{da^{(n)}}{dy} \right|_{\pi R^+} - \left. \frac{da^{(n)}}{dy} \right|_{\pi R^-} = -r_G m_n^2 a^{(n)}(y)|_{\pi R}. \quad (16)$$

⁴Note that the non-linear term in F^{MN} , which is present if G_N is a non-abelian field, is considered a part of the interaction.

Notice the total similarity between the equation of motion and the boundary conditions for a gauge field – eqns. (14) - (16) – and those found earlier for a fermion field as given in eqns. (5) - (7). It is but natural that the wave-functions for the gauge fields can be written down from those for the fermions by appropriate substitutions.

It is straightforward to verify that the masses m_n in eqn. (14) are solutions of:

$$(r_G^2 m_n^2 - 4) \tan(m_n \pi R) = 4 r_G m_n . \quad (17)$$

Eqn. (9) satisfied by KK fermions and eqn. (17) valid for KK gauge bosons are of identical form. Though we do not show it here, it applies to the five-dimensional scalar fields as well. We will next discuss solutions of transcendental equations of this type. These solutions are the masses of the KK-excitations if the zero-mode is taken massless⁵, to be compared with n/R for UED. In our discussion below we will use for the BLKT parameter the general notation r rather than r_f, r_G , etc. It is convenient to define the dimensionless variables

$$M_{(n)} \equiv m_n R \text{ and } R_{BLKT} \equiv r/R \quad (18)$$

in terms of which eqs. (9) and (17) can be cast in the form:

$$\left(R_{BLKT}^2 M_{(n)}^2 - 4 \right) \tan(\pi M_{(n)}) = 4 R_{BLKT} M_{(n)} \quad (19)$$

which can be readily reexpressed in the factorized form:

$$\left[R_{BLKT} M_{(n)} + 2 \tan\left(\frac{\pi M_{(n)}}{2}\right) \right] \left[R_{BLKT} M_{(n)} - 2 \cot\left(\frac{\pi M_{(n)}}{2}\right) \right] = 0 \quad (20)$$

It is easy to convince oneself that the solutions for even n arise from the first factor while those for odd n follow from the second. The zero mode is the trivial solution from the first factor and receives no contributions from the BLKT.

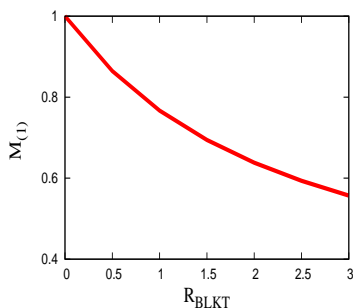


Figure 1: Variation of $M_{(1)} \equiv m_1 R$ with the BLKT strength $R_{BLKT} \equiv r/R$. The result applies to fermions, gauge bosons, and Higgs scalars when the BLKTs are symmetric. Note that larger R_{BLKT} yields a smaller mass.

Here we are interested only in the $n = 1$ KK modes. In Fig. 1, we plot $M_{(1)}$ as a function of R_{BLKT} as obtained from the second factor in eq. (20). For any chosen R_{BLKT} there is a unique

⁵As discussed below, the KK modes also receive a contribution to their masses from spontaneous breaking of the electroweak symmetry.

$M_{(1)} = m_1 R$. When we display the results in the later sections we present figures where R_B is held fixed and the mass $m_{B^{(1)}}$ is varied by changing $1/R$. Note that when $R_{BLKT} = 0$, i.e., no BLKT at all, one gets $m_1 = R^{-1}$, as expected. Further m_1 monotonically decreases as the BLKT strength, R_{BLKT} , increases. Obviously, the LKP will correspond to the $n = 1$ KK excitation of the field with the largest BLKT parameter.

In this work we concentrate on bosonic LKP states; this can be either $W_3^{(1)}$ or $B^{(1)}$. From our discussion it is clear that $M_{(1)}$ is determined entirely by the BLKT parameter, R_{BLKT} , and the compactification radius R . The gauge coupling is not involved. Therefore the earlier discussion applies for both $W_3^{(1)}$ and $B^{(1)}$ so long as the appropriate BLKT parameters are used. Which one of these happens to be the LKP is determined entirely by the choice of the respective BLKT parameters. In the subsequent sections we investigate the prospects of these WIMPs playing the role of the dark matter particle.

We have not included the zero-mode masses in our consideration till now. We indicate next how they affect the masses and mixing of $W_3^{(1)}$ and $B^{(1)}$. The electroweak gauge boson eigenstates in a five-dimensional theory with BLKT have been discussed in the literature [36]. We have verified that for the range of BLKT parameters which we consider the states of different KK level, n , mix negligibly. Further, only if the BLKT parameters for the B and W gauge bosons are exactly equal (or very nearly so) the mixing between $B^{(1)}$ and $W_3^{(1)}$ is substantial, it being equal to the zero-mode weak mixing angle in the case of equality. If $(r_B - r_W)/R$ is of order 0.1 (or larger) this mixing is negligible. This can be verified from the mass matrix which we now discuss.

The mass matrix for the $n = 1$ neutral electroweak gauge bosons including spontaneous breaking of electroweak symmetry as well as the extra-dimensional contribution discussed above is⁶:

$$M_{W_3^{(1)} B^{(1)}} = \begin{pmatrix} \frac{g_2^2 v_0^2}{4} \frac{S_W}{S_H} I_{W_3 W_3} + m_{W_3^{(1)}}^2 & -\frac{g_2 g_1 v_0^2}{4} \frac{\sqrt{S_W S_B}}{S_H} I_{W_3 B} \\ -\frac{g_2 g_1 v_0^2}{4} \frac{\sqrt{S_W S_B}}{S_H} I_{W_3 B} & \frac{g_1^2 v_0^2}{4} \frac{S_B}{S_H} I_{B B} + m_{B^{(1)}}^2 \end{pmatrix}, \quad (21)$$

where

$$I_{ij} = \int_0^{\pi R} (1 + r_h \{\delta(y) + \delta(y - \pi R)\}) a_i^{(1)}(y) a_j^{(1)}(y) dy, \quad (i, j = W_3, B). \quad (22)$$

Above, r_h is the strength of the Higgs scalar BLKT and $R_h = r_h/R$. Also,

$$a_{W_3}^{(1)}(y) = N_{W_3}^{(1)} \left[\cos(m_{W_3^{(1)}} y) - \frac{r_W m_{W_3^{(1)}}}{2} \sin(m_{W_3^{(1)}} y) \right], \quad (23)$$

and

$$a_B^{(1)}(y) = N_B^{(1)} \left[\cos(m_{B^{(1)}} y) - \frac{r_B m_{B^{(1)}}}{2} \sin(m_{B^{(1)}} y) \right], \quad (24)$$

with $N_{W_3}^{(1)}$, $N_B^{(1)}$ being normalisation factors as in eqn. (11).

The five-dimensional gauge couplings \hat{g}_2, \hat{g}_1 and the vacuum expectation value (vev) v_5 are related to the four-dimensional couplings g_2, g_1 respectively and the vev v_0 through

$$\hat{g}_2 = g_2 \sqrt{\pi R S_W}, \quad \hat{g}_1 = g_1 \sqrt{\pi R S_B}, \quad v_5 = v_0 / \sqrt{\pi R S_H}, \quad (25)$$

⁶Here $m_{W_3^{(1)}}$ and $m_{B^{(1)}}$ stand for the extra-dimensional mass contribution m_1 , discussed above, for the $n = 1$ W_3 and B states, respectively.

where

$$S_W = \left(1 + \frac{R_W}{\pi}\right), \quad S_B = \left(1 + \frac{R_B}{\pi}\right), \quad S_H = \left(1 + \frac{R_h}{\pi}\right). \quad (26)$$

A few comments about the mass matrix in eqn. (21) are in order. The matrix is given in the $W_3^{(1)} - B^{(1)}$ basis⁷. To estimate the relative magnitudes of the terms notice that the S_i are $\mathcal{O}(1)$ as are the overlap integrals I_{ij} . Therefore the contributions to the mass matrix from the symmetry breaking are $\mathcal{O}(v_0^2)$. The extra-dimensional contributions, $m_{G^{(1)}}^2$, are of the order of $(1/R)^2$ and are always dominant by far. As a consequence these terms determine the mass eigenvalues and the mixing is negligible for $(R_W - R_B) \sim 0.1$ or larger⁸. So, in our discussion below we take $B^{(1)}$ and $W_3^{(1)}$ to be the neutral electroweak gauge eigenstates. The contributions to the masses themselves from electroweak symmetry breaking are insignificant and hence dropped. We have verified that for the cases of our interest there is no significant dependence of the results on the Higgs scalar BLKT strength, r_h . In our calculations we keep $R_h = 0.1$ throughout.

III Standard calculation of relic density

In this section we briefly summarize the standard calculation of relic density. This will facilitate us in defining the notations as well as to put the calculation in the nmUED model in a proper context. For a more detailed elaboration of this formulation the reader is referred to [15, 17].

Let us consider the spectrum of the $n = 1$ KK-level of nmUED in which the particles are specified by $\alpha_i, (i = 0, 1, 2, \dots)$ ordered sequentially in mass. α_0 is identified with $B^{(1)}$, which is the lightest⁹ of these states and hence stable. It is also massive and weakly interacting. Consequently it is a natural candidate for being the dark matter WIMP. Apart from α_0 all other particles are unstable and ultimately decay to $B^{(1)}$ in association with SM particles. Thus from any number N_i of α_i particles we end up getting exactly $N_i \alpha_0$ at the end of the decay chain. Consequently, to determine the relic density of α_0 it would be meaningful to study the evolution of $n (\equiv \sum_i n_i)$ instead of each number density n_i separately.

The evolution (with time or temperature) of the number density n is governed by the Boltzmann transport equation:

$$\frac{dn}{dt} = -3Hn - \langle \sigma_{eff} v \rangle (n^2 - n_{eq}^2). \quad (27)$$

here H is the Hubble parameter and n^{eq} the number density at thermal equilibrium. $\langle \sigma_{eff} v \rangle$ is the thermally averaged relative velocity times the effective interaction cross section of α_0 with other particles in the spectra.

⁷We have checked that mixing with states of $n \neq 1$ is very small.

⁸If $R_W = R_B$ then the dominant diagonal terms are equal and do not affect the mixing and simply make a constant shift of the masses of the eigenstates. In this case the mixing between $W_3^{(1)}$ and $B^{(1)}$ is just as in the Standard Model with $\tan \theta = g'/g$.

⁹In nmUED, one has the flexibility to arrange $W_3^{(1)}$ or $\nu^{(1)}$ or $H^{(1)}$ to be the LKP. In this work we consider only the $W_3^{(1)}$ or $B^{(1)}$ as the dark matter candidate. In this section we stick to the $B^{(1)}$ LKP case.

$B^{(1)}$ annihilation	$B^{(1)}$ -lepton scattering
$B^{(1)}B^{(1)} \rightarrow f\bar{f}$	$\nu_L^{(1)}B^{(1)} \rightarrow W^+l^-$
$B^{(1)}B^{(1)} \rightarrow h^+h^-$	$\bar{\nu}_L^{(1)}B^{(1)} \rightarrow W^-l^+$
	$\nu_L^{(1)}B^{(1)} \rightarrow Z\nu_l$
	$\bar{\nu}_L^{(1)}B^{(1)} \rightarrow Z\bar{\nu}_l$
	$l_L^{(1)-}B^{(1)} \rightarrow W^-\nu_l$
	$l_L^{(1)+}B^{(1)} \rightarrow W^+\bar{\nu}_l$
	$l_L^{(1)-}B^{(1)} \rightarrow Zl^-$
	$l_L^{(1)+}B^{(1)} \rightarrow Zl^+$

Table 1: The $B^{(1)}$ annihilation and $B^{(1)}$ -lepton scattering processes which contribute to the relic density calculation. The cross sections involve, besides the SM couplings, the vertices in secs. A.1.2, A.1.3, and A.1.1.

More precisely, σ_{eff} can be defined as,

$$\sigma_{eff}(x) = \frac{1}{g_{eff}^2} \sum_{ij}^N \sigma_{ij} F_i F_j, \quad (28)$$

with

$$F_i(x) = g_i(1 + \Delta_i)^{3/2} \exp(-x\Delta_i) \text{ and } g_{eff}(x) = \sum_{i=1}^N F_i. \quad (29)$$

Here

$$\Delta_i = \frac{m_i - m_0}{m_0}, \quad x = \frac{m_0}{T}, \quad (30)$$

with $\sigma_{ij} \equiv \sigma(\alpha_i\alpha_j \rightarrow SM)$ and g_i is the number of degrees of freedom for the particle α_i taking part in the annihilation or coannihilation process.

The right-hand-side of eqn. (27) has two terms. The first (proportional to H) accounts for the reduction of the number density due to the expansion of the universe, and the second one for the decrease (increase) of n_i due to its interaction with the other particles present in the spectrum.

It has been noted [15, 17] that in case all the Δ_i are larger than 10% σ_{eff} can be well estimated by calculating only the annihilation of α_0 with its own anti-particle to SM particles. The co-annihilation (processes involving other KK-particles which cascade decay ultimately to the LKP) contribution is important only when one or more Δ_i are less than 10%.

In the non-relativistic limit (which is appropriate in our calculation as we are interested to calculate the number density in an epoch when average temperature is less than the mass of the WIMP) one can use the approximation $\langle\sigma_{eff}v\rangle \sim a_{eff}(x) + b_{eff}(x)v^2 + \mathcal{O}(v^4)$.

After calculating the relevant σ_{ij} one can numerically integrate eqn. (27) to obtain the number density of the DM particle at the present epoch. Instead, here we use an approximate formula [15] for the number density (normalised to the critical density at the present epoch) given by:

$$\Omega_\alpha h^2 \approx \frac{1.04 \times 10^9 / 1\text{GeV}}{M_{Pl}} \frac{x_F}{\sqrt{g_*(x_F)}} \frac{1}{I_a + 3I_b/x_F}, \quad (31)$$

ν^1 annihilation and scattering	l^1 annihilation and scattering
$\nu_l^{(1)} \bar{\nu}_l^{(1)} \rightarrow f \bar{f}$	$l_L^{(1)+} l_L^{(1)-} \rightarrow h^+ h^-$
$\nu_l^{(1)} \bar{\nu}_l^{(1)} \rightarrow h^+ h^-$	$l_L^{(1)+} l_L^{(1)-} \rightarrow ZZ + Z\gamma + \gamma\gamma$
$\nu_l^{(1)} \bar{\nu}_l^{(1)} \rightarrow ZZ$	$l_L^{(1)+} l_L^{(1)-} \rightarrow W^+ W^-$
$\nu_l^{(1)} \bar{\nu}_l^{(1)} \rightarrow W^+ W^-$	$l_L^{(1)\pm} l_L^{(1)\pm} \rightarrow l^\pm l^\pm$
$\nu_l^{(1)} \nu_l^{(1)} \rightarrow \nu_l \nu_l$	$l_L^{(1)\pm} l_L^{(1)\pm} \rightarrow l^\pm l'^\pm$
$\nu_l^{(1)} \nu_{l'}^{(1)} \rightarrow \nu_l \nu_{l'}$	$l_L^{(1)\pm} l_L^{(1)\mp} \rightarrow l^\pm l'^\mp$
$\nu_l^{(1)} \bar{\nu}_{l'}^{(1)} \rightarrow \nu_l \bar{\nu}_{l'}$	$l_L^{(1)+} l_L^{(1)-} \rightarrow f \bar{f} \text{ or } l_R^+ l_R^-$
$\nu_l^{(1)} \bar{\nu}_{l'}^{(1)} \rightarrow l^- l'^+$	$l_L^{(1)+} l_L^{(1)-} \rightarrow \nu_l \bar{\nu}_{l'} \text{ or } l_L^+ l_L^-$
$\nu_l^{(1)} \bar{\nu}_l^{(1)} \rightarrow l^+ l^-$	$l_L^{(1)} \bar{l}_L^{(1)'} \rightarrow \nu_l \bar{\nu}_{l'}$

Table 2: The $\nu^{(1)}$ and $l^{(1)}$ annihilation and scattering processes which contribute to the relic density calculation. The cross sections involve, besides the SM couplings, the vertices in secs. A.1.1 and A.1.5.

where M_{Pl} is the Planck mass and

$$I_a = x_F \int_{x_F}^{\infty} a_{eff}(x) x^{-2} dx, \quad (32)$$

$$I_b = 2x_F^2 \int_{x_F}^{\infty} b_{eff}(x) x^{-3} dx. \quad (33)$$

Here x_F is the freeze-out temperature and can be solved from the following equation,

$$x_F = \ln \left(\frac{15}{8} \sqrt{\frac{5}{2}} \frac{g_{eff}(x_F)}{2\pi^3} \frac{m_0 M_{Pl} [a_{eff}(x_F) + 6b_{eff}(x_F) x_F^{-1}]}{\sqrt{g_*(x_F) x_F}} \right). \quad (34)$$

Above, $g_*(x_F)$ accounts for the relativistic degrees of freedom at the freeze-out temperature for which we have used the value of 92. For the parameter ranges used in this analysis x_F is found to be around 23 - 26.

At this point, given a model one is well-equipped to calculate the relic particle density. In UED (also in nmUED) there are two main classes of reactions which contribute to σ_{eff} ; namely, the annihilation of relic particles into the SM particles and the co-annihilation processes (explained above). It is to be noted that in UED the mass spectrum depends only on one parameter R^{-1} . In contrast, in nmUED masses of the KK-excitations have strong dependence on all the BLKT parameters. Thus it is the choice of the BLKT parameters which determines whether or not the mass of any KK-excitation would lie close to the relic particle mass ($\Delta_i \leq 10\%$) so that their co-annihilation process could contribute significantly. In our analysis we have chosen the BLKT parameters for quarks, gluons and right-handed leptons such that their masses are sufficiently larger than the $B^{(1)}$ mass and their contributions to co-annihilation are negligible. For this choice only the coannihilation of KK-excitations of the left-handed lepton doublets are relevant.

In Tables 1 - 3 we have listed the reactions which are used to calculate σ_{eff} . Some of the couplings among the $n = 1$ KK-modes and SM particles get modified in nmUED due to the non-trivial wave-functions of the KK-excitations in the fifth-dimension. (We have listed such interactions with the Feynman rules in Appendix A.) Consequently, the cross sections of some of the processes contributing in σ_{eff} will be accordingly scaled up or down with respect to their UED values.

$\nu^{(1)}-l^{(1)}$ scattering	
$\nu_L^{(1)} l_L^{(1)'} \rightarrow \nu_l l'$	$l_L^{(1)-} \bar{\nu}_L^{(1)} \rightarrow f \bar{f}'$
$l_L^{(1)-} \bar{\nu}_L^{(1)} \rightarrow h^- h^0$	$l_L^{(1)-} \bar{\nu}_L^{(1)} \rightarrow \gamma W^-$
$l_L^{(1)-} \bar{\nu}_L^{(1)} \rightarrow ZW^-$	$l_L^{(1)-} \bar{\nu}_L^{(1)} \rightarrow l^- \bar{\nu}_l$
$l_L^{(1)-} \nu_L^{(1)} \rightarrow l^- \nu_l$	$\nu_L^{(1)} l_L^{(1)'} \rightarrow \nu_l l'^-$
$\nu_L^{(1)} l_L^{(1)'} \rightarrow \nu_l l'^-$	$\bar{\nu}_L^{(1)} l_L^{(1)'} \rightarrow \bar{\nu}_l l'^-$

Table 3: The $\nu^{(1)} - l^{(1)}$ scattering processes which contribute to the relic density calculation. The cross sections involve, besides the SM couplings, the vertices in secs. A.1.1 and A.1.5.

IV Dark Matter relic density in nmUED

We are now ready to present the results and compare it with the current observed value¹⁰ of Ωh^2 from Planck data [1]. A similar exercise in the framework of UED (when $B^{(1)}$ is the candidate for dark matter) yields a narrow range¹¹ [17] of allowed values – 500 - 600 GeV – for the compactification scale R^{-1} . However we will see that in nmUED this bound on R^{-1} will be relaxed significantly¹². We take up the cases of $B^{(1)}$ and $W_3^{(1)}$ LKP separately.

IV.1 Results for $B^{(1)}$ LKP

$B^{(1)}$ is an oft-chosen dark matter candidate in UED. Here for this choice we use the modifications in the mass spectrum and the couplings to estimate the relic density in nmUED. In Fig. 2 we present the main outcome of this analysis where in the three panels R_B is chosen differently. Variation of Ωh^2 (with the mass of $B^{(1)}$) has been plotted for different choices of the fermion BLKT parameter, R_f . As noted above, the BLKT parameters for quarks, gluons and right-handed fermions is so chosen that the masses of these KK-excitations are well above that of the $B^{(1)}$. So, they play no role in the determination of relic density. Furthermore, we have checked that Ωh^2 is nearly insensitive to the choice of r_h , the Higgs BLKT parameter.

It may not be out of place to make a comment about the choice of parameter values in the plots in Fig. 2. In each panel R_B has a fixed value. Thus $m_{B^{(1)}}$ is being varied along the x -axes by changing R^{-1} . To ensure that $B^{(1)}$ is the LKP, $n = 1$ KK-lepton masses should be greater than $m_{B^{(1)}}$; consequently, R_f (chosen same for all three left-handed lepton doublets) must be smaller than R_B in every panel. In each panel, we also show the values of Δ_f corresponding to five (equi-spaced) choices of R_f .

It would be useful to remark that while calculating σ_{eff} we have taken $l_L^{(1)}$ and $\nu_L^{(1)}$ as mass degenerate and they are the next heavier in mass than the LKP assuming all other KK modes being heavy enough so that their contribution can be neglected. For a given value of R^{-1} , we find that the cross sections of the reactions listed in Tables 1 - 3 are higher compared to the corresponding rates in UED. Relatively lower values of the $n = 1$ KK-masses and enhanced couplings in nmUED account for the higher

¹⁰We use of $\Omega h^2 = 0.1198 \pm 0.0026$, the 1σ results from Planck.

¹¹It has been pointed out [40] that if the contributions from $n=2$ excitations are included then this limit is pushed up above 1 TeV.

¹²We also make remarks in passing about the constraint set on the LKP mass or equivalently the compactification scale by the limit from overclosure of the universe.

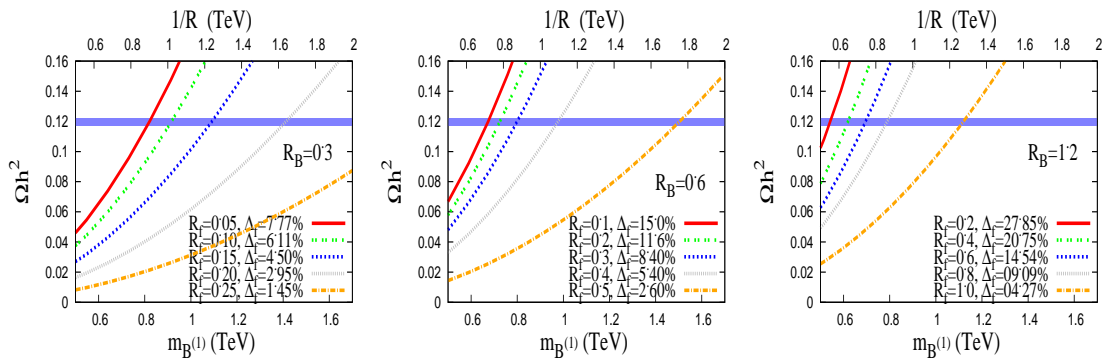


Figure 2: Variation of Ωh^2 with relic particle mass. Curves for different choices of the fermion BLKT parameter R_f are shown and the corresponding Δ_f indicated. The narrow horizontal blue band corresponds to the 1σ allowed range of relic particle density from Planck data. The allowed $1/R$ can be read off from the intersections of the curves with the allowed band. The three panels are for different choices of R_B , the BLKT parameter for B .

reaction rates for a given value of R^{-1} . Consequently, the numerical value of the relic density in nmUED is always less than in UED as long as the BLKT parameters are positive (as used in this analysis).

It is possibly useful to mention here the magnitudes of the coefficients I_a and I_b in eqn. (31) which reflect the model dynamics. For the R_B and R_f considered by us I_a and I_b are in the range of (1 - 10) pb . Both I_a and I_b decrease with increasing $m_{B(1)}$.

One can see from Fig. 2 that Ωh^2 increases with increase of R^{-1} or R_B . (Both increases serve to reduce $m_{B(1)}$ and also enhance the couplings.) In contrast, Ωh^2 decreases with increasing R_f , the fermion BLKT coefficient. Unlike in UED, the allowed range of R^{-1} depends on R_f in this non-minimal version of the model. This is in line with expectation. As R_f moves away from R_B the splitting, Δ_f , increases (noted in the figures) and coannihilation becomes less important.

It is seen from Fig. 2 that depending on the choice of R_B and R_f the allowed range of R^{-1} can be as much as 0.6 TeV to 2 TeV or even more, while remaining consistent with the observed dark matter limits. It should be borne in mind that in nmUED the *mass* of the LKP is actually a little *lower* than R^{-1} as seen in the lower x -axes in the panels.

In passing we remark on the upper bounds on R^{-1} that arise by demanding that the LKP does not overclose the universe. For this to happen Ωh^2 must be around 0.48. Some sample results are presented in Table 4. To be conservative, for every R_B we have chosen the smallest R_f (i.e., the largest Δ_f) in Fig. 2. For larger R_f the upper bound on R^{-1} is increased.

The observed 1σ limits of Ωh^2 , which we have used, are very restrictive. In Fig. 3 we have presented the regions in the $m_{B(1)}-m_{f(1)}$ plane which leads to Ωh^2 in the observed range. While deriving these limits we assume that $B^{(1)}$ is the *only* relic particle in the model. Fig. 3 points to very narrow regions in the $m_{B(1)} - m_{f(1)}$ plane – *between* the two curves in each panel – allowed by the data. Thanks to the present precision of cosmological measurements, when translated to the $m_{B(1)}-m_{f(1)}$ plane one has essentially reduced the allowed range to almost a line. The plots in Fig. 3 reveal that the allowed

LKP	R_B or R_W	R_f	Δ_f	R^{-1} (in TeV)	$m_{B^{(1)}}$ or $m_{W_3^{(1)}}$ (in TeV)
$B^{(1)}$	0.3	0.05	7.7%	1.9	1.7
	0.6	0.1	15%	1.7	1.4
	1.2	0.2	27.8%	1.5	1.1
$W_3^{(1)}$	0.6	-	-	10.0	8.4

Table 4: Upper bound on R^{-1} from overclosure of the universe ($\Omega h^2 = 0.48$). The mass of the LKP for the limiting R^{-1} is also presented. For the $W_3^{(1)}$ LKP case only the process $W_3^{(1)} W_3^{(1)} \rightarrow W^+ W^-$ is taken into account. Including coannihilation will further enhance the upper bound in this case.

range is very close to the $m_{B^{(1)}} = m_{f^{(1)}}$ line. (We are not interested in the region above this line, where $f^{(1)}$ becomes the LKP.)

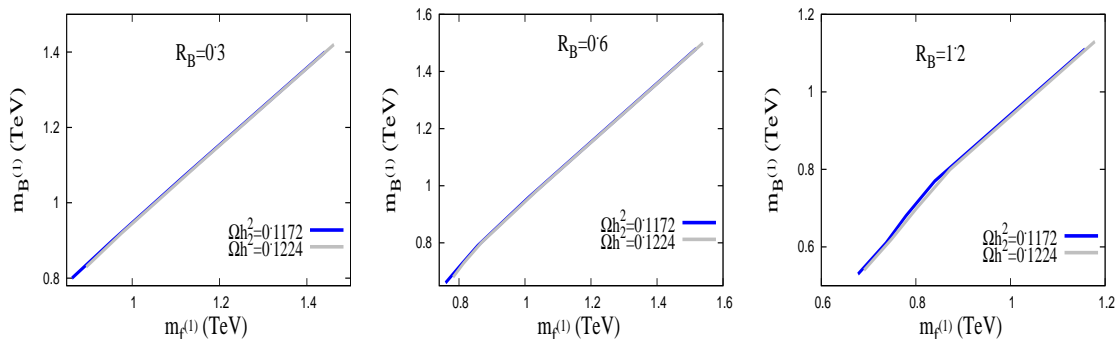


Figure 3: Allowed region in the $m_{f^{(1)}} - m_{B^{(1)}}$ plane that satisfies the observed Ωh^2 limits. The three panels are for different choices of R_B . Only the narrow strip *between* the two curves is allowed from the relic density constraints.

IV.2 What if $W_3^{(1)}$ is the LKP?

The masses of the $n = 1$ KK-states are determined by their respective BLKT parameters r_i or equivalently $R_i = r_i/R$. To avoid a fermion LKP we always choose $R_B, R_W > R_f$. Besides the just discussed case of $R_B > R_W$, corresponding to $B^{(1)}$ being the LKP, one should also consider $R_W > R_B$ which makes $W_3^{(1)}$ the dark matter candidate¹³. In such an event we find that the annihilation cross section is large (notably because of the process $W_3^{(1)} W_3^{(1)} \rightarrow W^+ W^-$) and therefore the relic density is too small¹⁴. The relic density as a function of the $W_3^{(1)}$ mass is shown in Fig. 4 for a typical value of $R_W = 0.6$. Note that the obtained density is far below the observed [1] value (around 0.12). For $R_W = 0.6$ the lower (upper) bounds on Ωh^2 – which are outside the range of the figure – correspond to $R^{-1} = 4.66$ (4.7) TeV with the respective $W_3^{(1)}$ masses 3.92 (4.04) TeV. This establishes that $W_3^{(1)}$ would not be an attractive dark matter candidate for easy detection at the LHC unless the DM has

¹³For a different discussion of the $W_3^{(1)}$ LKP see, for example, [41].

¹⁴We have not considered coannihilation in this case. It would further reduce the relic density.

several components¹⁵.

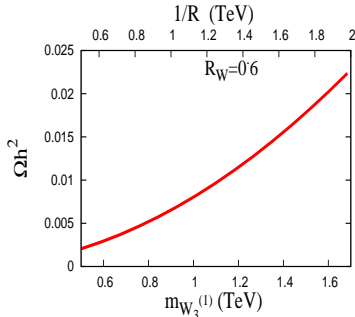


Figure 4: Variation of the relic density with $m_{W_3^{(1)}}$ when $W_3^{(1)}$ is identified as the DM candidate. The current observed value (~ 0.12) disfavors this alternative.

V Direct detection of nmUED relic particle

Finally, we would like to take a look at the prospects of direct detection of $B^{(1)}$ at an experiment such as XENON [42]. We will not estimate the actual event rates at such an experiment; instead, the spin dependent and spin independent cross sections of $B^{(1)}$ scattering off Xenon nuclei ($A = 131$, $Z = 54$) will be estimated. Event rates and cross sections of dark matter in the context of UED have been obtained in ref. [43, 44]. As masses and also the couplings in nmUED show a distinctive departure from the corresponding quantities in UED, we wish to relook at the calculation.

The cross section of scattering of dark matter off nuclei such as Xenon is ultimately related to its scattering from quarks. As is customary, we use the non-relativistic limit to separate the spin-independent (i.e., scalar) and spin-dependent parts of the cross section.

The scalar part of the scattering cross section of $B^{(1)}$ with a nucleus of mass m_N with atomic number Z and mass number A at zero momentum transfer is given by

$$\sigma_0^{scalar} = \frac{m_N^2}{4\pi(m_{B^{(1)}} + m_N)^2} \left(Z f_p^{B^{(1)}} + (A - Z) f_n^{B^{(1)}} \right)^2, \quad (35)$$

where

$$f_{p,n}^{B^{(1)}} = m_{p,n} \sum_q \frac{\gamma_q + \beta_q}{m_q} f_{T_q}^{(p,n)}. \quad (36)$$

In our numerical evaluations we have used $f_{T_q}^{(p,n)} = \langle q\bar{q} \rangle_{p,n}(m_q/m_{p,n})$, which relate the quark-level cross sections to that for the nucleons, as given in [8]. The physics of the specific dark matter candidate is captured in the quantities γ_q and β_q which here stand for the interaction of $B^{(1)}$ with quarks mediated via the SM Higgs exchange and $n = 1$ KK-fermion exchange respectively. We find

$$\gamma_q = -\frac{g_1^2 m_q}{2 m_h^2}, \quad \text{and} \quad \beta_q = -m_q \frac{\tilde{g}_1^2 (Y_{qL}^2 + Y_{qR}^2)}{(m_{B^{(1)}}^2 - m_{q^{(1)}}^2)^2} (m_{B^{(1)}}^2 + m_{f^{(1)}}^2). \quad (37)$$

¹⁵The overclosure bound on R^{-1} for $R_W = 0.6$ is 10 TeV (see Table 4).

where

$$g_1'^2 = g_1^2 \pi R \left(1 + \frac{R_B}{\pi} \right) \frac{1}{\sqrt{1 + \frac{R_h}{\pi}}} I_{B^{(1)}B^{(1)}h^{(0)}} \quad (38)$$

where $I_{B^{(1)}B^{(1)}h^{(0)}}$ is given in eqn. A-4.

$$\tilde{g}_1 = g_1 \sqrt{\pi R \left(1 + \frac{R_B}{\pi} \right)} I_{B^{(1)}f^{(1)}f^{(0)}} \quad (39)$$

with $I_{B^{(1)}f^{(1)}f^{(0)}}$ given in eqn. A-1. Numerically γ_q is almost insensitive to $m_{B^{(1)}}$ and about two orders of magnitude larger than β_q .

The corresponding spin-dependent cross section is given by:

$$\sigma_0^{spin} = \frac{2}{3\pi} (\mu^2 \tilde{g}_1^4) \left(\frac{a_p \langle S_p \rangle + a_n \langle S_n \rangle}{m_{B^{(1)}}^2 - m_{q^{(1)}}^2} \right)^2 \frac{(J+1)}{J} \quad (40)$$

where μ is the reduced mass of the target nucleus and the the other nuclear parameters can be found in [8]. In particular,

$$a_p = \frac{17}{36} \Delta u + \frac{5}{36} (\Delta d + \Delta s) \quad \text{and} \quad a_n = \frac{17}{36} \Delta d + \frac{5}{36} (\Delta u + \Delta s) \quad (41)$$

Following ref. [43], in our analysis we have used the central values of $\Delta u = 0.78 \pm 0.02$, $\Delta d = -0.48 \pm 0.02$ and $\Delta s = -0.15 \pm 0.02$.

Experimental results are often presented in terms of *effective* dark matter - nucleon scattering cross sections given by:

$$\begin{aligned} \sigma_{p,n}^{scalar} &= \sigma_0 \frac{m_{p,n}^2}{\mu^2} \frac{1}{A^2} \cdot \cdot, \\ \sigma_{p,n}^{spin} &= \frac{\tilde{g}_1^4}{2\pi} \frac{\mu_{p,n}^2 a_{p,n}^2}{(m_{B^{(1)}}^2 - m_{f^{(1)}}^2)^2} \end{aligned} \quad (42)$$

Here, $\mu_{p,n}$ is the reduced mass of the WIMP-nucleon system.

We can now turn to the numerical results for the spin-dependent and scalar WIMP-nucleon cross section for Xenon. The cross sections will be presented as a function of the LKP ($B^{(1)}$) mass which is fixed by R^{-1} and the BLKT parameter R_B . We will restrict R_f the lepton BLKT strength to only those values which satisfy the relic density Ωh^2 requirement once R_B is fixed; i.e., the range shown in Fig. 3. To appreciate this choice of input parameters we refer to Fig. 2. For a fixed value of R_B (i.e., any one panel) and R_f (one of the curves in the panel) one has two values of R^{-1} resulting from the 1σ upper and lower allowed values of Ωh^2 . For each such R_B, R_f pair the (two) R^{-1} values have been used to present the direct detection cross section bands in Figs. 5 and 6. Thus as we go along left to right along x -axis of these plots, R_f increases along with $m_{B^{(1)}}$.

Scattering rates of the the LKP WIMP off nucleons are presented in Fig. 5 (scalar cross section, σ_n^{scalar}) and in Fig. 6 (spin dependent cross section, σ_n^{spin}). Over the range of input parameters we have considered, σ_n^{scalar} decreases by two orders of magnitude from 10^{-46} cm² to 10^{-48} cm² while σ_n^{spin} is around 10^{-42} cm² and is not very sensitive to the change of R^{-1} and R_f . It would be relevant here

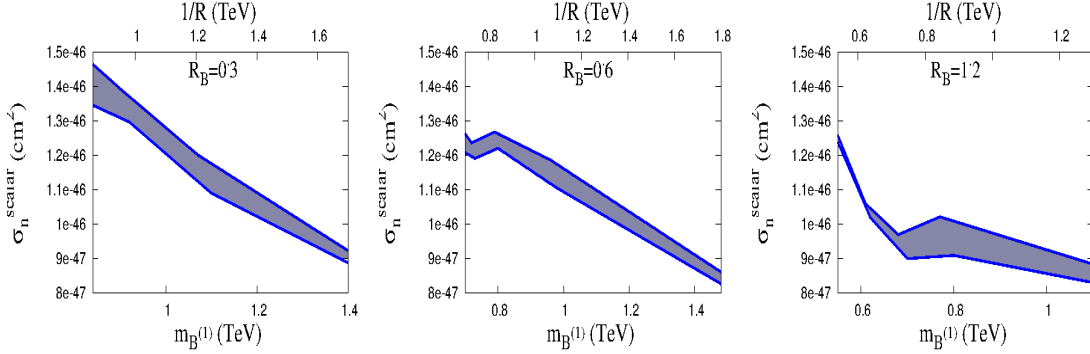


Figure 5: Variation of the spin independent WIMP nucleon cross section with relic particle mass for Xenon. The three panels are for three values of R_B . The shaded region is obtained by using the BLKT parameters consistent with the observed relic density.

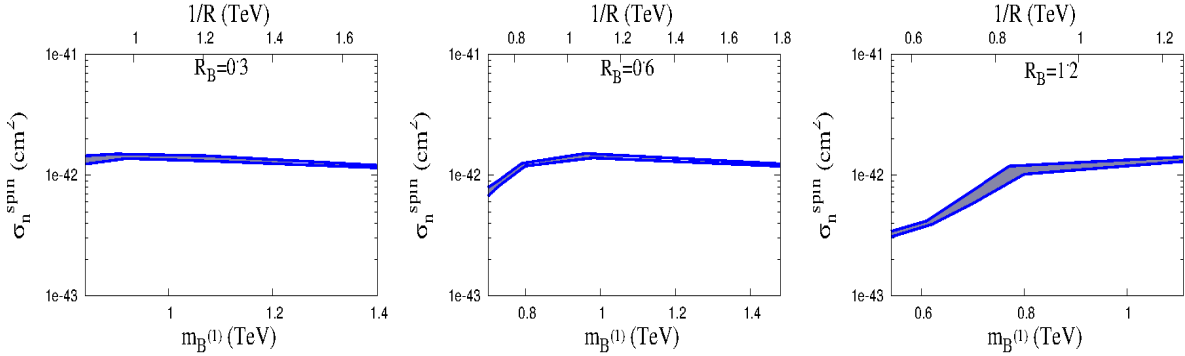


Figure 6: Variation of the spin dependent WIMP nucleon cross section with relic particle mass for Xenon. The three panels are for three values of R_B . The shaded region is obtained by using the BLKT parameters consistent with the observed relic density.

to mention that these values of the WIMP scattering cross sections are well below the sensitivity of the XENON experiment¹⁶. Thus the entire range of parameters used for the direct detection rates is allowed by the XENON experiment.

The plots in Figs. 5 and 6 for the dark matter cross sections appear somewhat different from those given for UED in [43] and [45]. The reason for this is that unlike in those analyses here the fermion KK-excitation masses and the $B^{(1)}$ mass are strongly correlated (see Fig. 3) by virtue of the requirement that the observed DM relic density be reproduced.

The nature of variation of the DM scattering cross sections as presented in Figs. 5 and 6 can be seen to follow from eqn. (42). BLKT parameter dependence creeps into σ_n^{spin} via the $\left(m_{f^{(1)}}^2 - m_{B^{(1)}}^2\right)^2$ factor in the denominator along with \tilde{g}_1 . \tilde{g}_1 is barely sensitive to R^{-1} or R_f . And so is the former: as

¹⁶For the range of WIMP masses in Fig. 5, sensitivity of the XENON experiment [42] for the scalar cross section is above 10^{-45} cm^2 [42].

we go from left to right along the x -axis, $(m_{f^{(1)}} - m_{B^{(1)}})$ decreases while $(m_{f^{(1)}} + m_{B^{(1)}})$ increases, making the cross section almost independent of $m_{B^{(1)}}$. On the other hand, the scalar cross section has a more complicated dependence on the BLKT parameters. While $\frac{\gamma_q}{m_q}$ is almost independent of BLKT parameters, $\frac{\beta_q}{m_q}$ increases with $m_{B^{(1)}}$ and R_f . However, the γ_q contribution dominates and thus the combination $\frac{(-\gamma_q - \beta_q)}{m_q}$ changes slowly with $m_{B^{(1)}}$ and R_f . An overall factor of $m_{B^{(1)}}^2$ in the denominator of σ_0 (see eqn. (35)), accounts for the rapid decrease of the scalar cross section, which falls monotonically in Fig. 5.

VI Summary and Conclusions

Universal Extra Dimension models have emerged as an attractive option for Beyond the Standard Model physics. In this model all SM particles are complemented with KK-excitations which are equispaced in mass. The interaction strengths of these states are determined entirely by the SM. Many aspects of the model ranging from constraints from precision measurements to collider searches have been examined in the literature. Signals for UED are being actively looked for at the LHC.

One of the less attractive predictions of UED is the mass degeneracy of KK-excitations of all SM particles at any fixed level. A remedy for this is not unknown. It has been shown [12] that five-dimensional radiative corrections split the degeneracy in a definite way determined by the SM charges of the zero-mode states. The corrections are encoded as contributions to the four-dimensional lagrangians located at the two fixed points of the orbifold. In this version of the model, known as minimal UED, the practice has been to assume that the couplings of the KK excitations continue to be as for the SM particles.

Our work is on a further generalisation of this model where the extra four-dimensional kinetic terms located at the two fixed points are of a strength which is a free parameter and varies from particle to particle. To ensure the conservation of a \mathbf{Z}_2 parity the strengths are taken equal at the two fixed points. This ensures the stability of the LKP. The BLKT parameters determine the wave-functions of the KK-excitations in the fifth dimension, y , as well as their masses. Further, the non-trivial y -dependence of the wave-functions affects the couplings of the KK-excitations; these are also controlled by the BLKT parameters. We allow different BLKT strengths for the various SM particles and ensure that $B^{(1)}$ is the LKP. We also examine the alternative of a $W_3^{(1)}$ LKP but find that the relic density is too small for a WIMP mass ~ 1 TeV. We conclude that $W_3^{(1)}$ cannot serve the role of a single component dark matter when its mass is within the LHC range. We make a note of the bounds on the LKP dark matter particle mass which follow from the overclosure of the universe.

In this work we consider dark matter in this nmUED scenario retaining the impact of BLKT parameters on the masses *and* the couplings. We show that the range of relic densities preferred by the Planck data places stringent restrictions on the BLKT strengths of the gauge bosons and fermions and these get correlated. We find that in this process the allowed range of the compactification scale R^{-1} is much relaxed from its narrow UED prediction of 0.5-0.6 TeV .

We discuss the prospects of direct detection of the nmUED dark matter candidate keeping the relic density constraints in mind. As an example, we evaluate the spin-dependent and spin-independent scattering cross section of dark matter off Xenon nuclei. Our calculations indicate that the signal is

well below the existing limits set by XENON100 for spin-independent scattering.

Acknowledgements: The authors are grateful to Tirtha Sankar Ray for collaborating in the early stages of this work. U.K.D. and A.S. thank Kirtiman Ghosh for valuable discussions. A.D. acknowledges partial support from the DRS project sanctioned to the Department of Physics, University of Calcutta by the University Grants Commission. U.K.D. is supported by funding from the Department of Atomic Energy, Government of India for the Regional Centre for Accelerator-based Particle Physics, Harish-Chandra Research Institute (HRI). A.R. is partially funded by the Department of Science and Technology Grant No. SR/S2/JCB-14/2009. A.S. thanks the University Grants Commission for support.

Appendix A: $n = 1$ KK-excitation Feynman rules

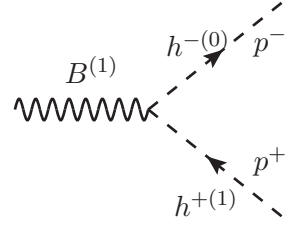
In this Appendix we note the Feynman rules for the $n = 1$ Kaluza-Klein excitations. Each of these vertices involves a nontrivial coupling determined by the five-dimensional wave-functions of the KK-excitations. These couplings are listed separately below. Besides these Feynman rules and couplings, only the SM rules are required.

A.1 Feynman Rules:

A.1.1 The $B^{(1)} f^{(1)} f^{(0)}$ vertex

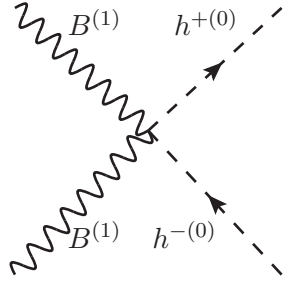
$$\equiv -i \left(g_1 \sqrt{\pi R \left(1 + \frac{R_B}{\pi} \right)} \times I_{B^{(1)} f^{(1)} f^{(0)}} \right) \gamma^\mu (P_L Y_L + P_R Y_R)$$

A.1.2 The $B^{(1)}h^{(1)}h^{(0)}$ vertex



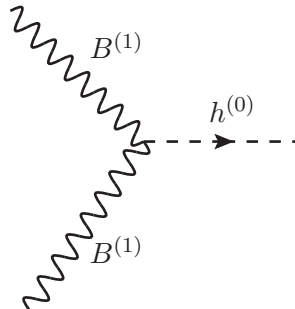
$$\equiv -i \left(g_1 \sqrt{\pi R \left(1 + \frac{R_B}{\pi} \right)} \times I_{B^{(1)}h^{+(1)}h^{-(0)}} \right) Y_H(p_\mu^- - p_\mu^+)$$

A.1.3 The $B^{(1)}B^{(1)}h^{(0)}h^{(0)}$ vertex



$$\equiv -2i \left(g_1^2 \pi R \left(1 + \frac{R_B}{\pi} \right) \times I_{B^{(1)}B^{(1)}h^{+(0)}h^{-(0)}} \right) \eta_{\mu\nu} Y_H^2$$

A.1.4 The $B^{(1)}B^{(1)}h^{(0)}$ vertex



$$\equiv -2i \left(g_1^2 \pi R \left(1 + \frac{R_B}{\pi} \right) \times I_{B^{(1)}B^{(1)}h^{(0)}} \right) \times \frac{v}{\sqrt{1 + \frac{R_h}{\pi}}} Y_H^2$$

A.1.5 The $W^{(1)} f^{(1)} f^{(0)}$ vertices

$$\begin{aligned} & \text{Diagram 1: } W_3^{(1)} \text{ vertex} \quad \equiv -i \left(g_2 \sqrt{\pi R \left(1 + \frac{R_W}{\pi} \right)} \times I_{W^{(1)} f^{(1)} f^{(0)}} \right) \gamma^\mu T_3 P_L \\ & \text{Diagram 2: } W^{+(1)} \text{ vertex} \quad \equiv -i \left(g_2 \sqrt{\pi R \left(1 + \frac{R_W}{\pi} \right)} \times I_{W^{(1)} f^{(1)} f^{(0)}} \right) \frac{\gamma^\mu}{\sqrt{2}} P_L \end{aligned}$$

A.2 Couplings:

Here we list the couplings which appear in the Feynman rules given above.

$$I_{B^{(1)} f^{(1)} f^{(0)}} = \int_0^{\pi R} [1 + r_f \{\delta(y) + \delta(y - \pi R)\}] a_B^{(1)} f^{(1)} f^{(0)} dy. \quad (\text{A-1})$$

$$I_{B^{(1)} h^{(1)} h^{(0)}} = \int_0^{\pi R} [1 + r_h \{\delta(y) + \delta(y - \pi R)\}] a_B^{(1)} h^{(1)} h^{(0)} dy. \quad (\text{A-2})$$

$$I_{B^{(1)2} h^{(0)2}} = \int_0^{\pi R} [1 + r_h \{\delta(y) + \delta(y - \pi R)\}] a_B^{(1)2} h^{(0)2} dy. \quad (\text{A-3})$$

$$I_{B^{(1)} B^{(1)} h^{(0)}} = \int_0^{\pi R} [1 + r_h \{\delta(y) + \delta(y - \pi R)\}] a_B^{(1)} a_B^{(1)} h^{(0)} dy. \quad (\text{A-4})$$

$$I_{W^{(1)} f^{(1)} f^{(0)}} = \int_0^{\pi R} [1 + r_f \{\delta(y) + \delta(y - \pi R)\}] a_W^{(1)} f^{(1)} f^{(0)} dy. \quad (\text{A-5})$$

where $a_B^{(n)}(y), f^{(n)}(y)$ are the the wave-functions for the gauge boson and fermion fields introduced earlier, and $h^{(n)}(y)$ is the same for the Higgs field.

References

- [1] P.A.R. Ade *et al.* [Planck Collaboration], arXiv:1303.5076[astro-ph.CO].
- [2] E. Komatsu *et al.* [WMAP Collaboration], *Astrophys. J. Suppl.* **192** (2011) 18 [arXiv:1001.4538 [astro-ph.CO]]; G. Hinshaw *et al.* [WMAP Collaboration], arXiv:1212.5226 [astro-ph.CO].

- [3] M. Aguilar *et al.* [AMS Collaboration], Phys. Rev. Lett. **110** (2013) 14, 141102.
- [4] D. Adriani, *et al.* [PAMELA Collaboration], Nature **458** (2009) 607 [arXiv:0810.4995 [astro-ph]].
- [5] M. Ackermann, *et al.* [Fermi LAT Collaboration], Phys. Rev. Lett. **108** (2012), 011103 [arXiv:1109.0521 [astro-ph.HE]].
- [6] G. Aad *et al.* [ATLAS Collaboration], Science **338** (2012) 1576.
- [7] S. Chatrchyan *et al.* [CMS Collaboration], Phys. Lett. B **710** (2012) 26 [arXiv:1202.1488 [hep-ex]].
- [8] G. Jungman, M. Kamionkowski and K. Griest, Phys. Rept. **267** (1996) 195 [arXiv:hep-ph/9506380].
- [9] A. Birkedal, A. Noble, M. Perelstein and A. Spray, Phys. Rev. D **74** (2006) 035002 [arXiv:hep-ph/0603077].
- [10] T. Appelquist, H. C. Cheng and B. A. Dobrescu, Phys. Rev. D **64** (2001) 035002 [arXiv:hep-ph/0012100].
- [11] H. Georgi, A. K. Grant and G. Hailu, Phys. Lett. B **506**, 207 (2001) [hep-ph/0012379].
- [12] H.C. Cheng, K.T. Matchev and M. Schmaltz, Phys. Rev. D **66** (2002) 036005 [arXiv:hep-ph/0204342].
- [13] H. C. Cheng, K. T. Matchev and M. Schmaltz, Phys. Rev. D **66** (2002) 056006 [arXiv:hep-ph/0205314].
- [14] R. N. Mohapatra and A. Perez-Lorenzana, Phys. Rev. D **67** (2003) 075015 [arXiv:hep-ph/0212254].
- [15] G. Servant and T. M. P. Tait, Nucl. Phys. B **650** (2003) 391; [arXiv: hep-ph/0206071].
- [16] D. Majumdar, Mod. Phys. Lett. A **18** (2003) 1705.
- [17] K. Kong and K. T. Matchev, JHEP **0601** (2006) 038, [arXiv: hep-ph/0509119].
- [18] F. Burnell and G. D. Kribs, Phys. Rev. D **73** (2006) 015001 [arXiv:hep-ph/0509118].
- [19] P. Dey and G. Bhattacharyya, Phys. Rev. D **70** (2004) 116012 [arXiv:hep-ph/0407314]; P. Dey and G. Bhattacharyya, Phys. Rev. D **69** (2004) 076009 [arXiv:hep-ph/0309110].
- [20] P. Nath and M. Yamaguchi, Phys. Rev. D **60** (1999) 116006 [arXiv:hep-ph/9903298].
- [21] D. Chakraverty, K. Huitu and A. Kundu, Phys. Lett. B **558** (2003) 173 [arXiv:hep-ph/0212047].
- [22] A.J. Buras, M. Spranger and A. Weiler, Nucl. Phys. B **660** (2003) 225 [arXiv:hep-ph/0212143]; A.J. Buras, A. Poschenrieder, M. Spranger and A. Weiler, Nucl. Phys. B **678** (2004) 455 [arXiv:hep-ph/0306158].
- [23] K. Agashe, N.G. Deshpande and G.H. Wu, Phys. Lett. B **514** (2001) 309 [arXiv:hep-ph/0105084].
- [24] J. F. Oliver, J. Papavassiliou and A. Santamaria, Phys. Rev. D **67** (2003) 056002 [arXiv:hep-ph/0212391].

- [25] T. Appelquist and H. U. Yee, Phys. Rev. D **67** (2003) 055002 [arXiv:hep-ph/0211023].
- [26] T.G. Rizzo and J.D. Wells, Phys. Rev. D **61** (1999) 016007 [arXiv:hep-ph/9906234]; A. Strumia, Phys. Lett. B **466** (1999) 107 [arXiv:hep-ph/9906266]; C.D. Carone, Phys. Rev. D **61** (1999) 015008 [arXiv:hep-ph/9907362].
- [27] I. Gogoladze and C. Macesanu, Phys. Rev. D **74** (2006) 093012 [hep-ph/0605207].
- [28] T. Rizzo, Phys. Rev. D **64** (2001) 095010 [arXiv:hep-ph/0106336]; C. Macesanu, C.D. McMullen and S. Nandi, Phys. Rev. D **66** (2002) 015009 [arXiv:hep-ph/0201300]; Phys. Lett. B **546** (2002) 253 [arXiv:hep-ph/0207269]; H.-C. Cheng, Int. J. Mod. Phys. A **18** (2003) 2779 [arXiv:hep-ph/0206035]; A. Muck, A. Pilaftsis and R. Rückl, Nucl. Phys. B **687** (2004) 55 [arXiv:hep-ph/0312186]; B. Bhattacharjee and A. Kundu, J. Phys. G **32**, 2123 (2006) [arXiv:hep-ph/0605118]; B. Bhattacharjee and A. Kundu, Phys. Lett. B **653**, 300 (2007) [arXiv:0704.3340 [hep-ph]]; G. Bhattacharyya, A. Datta, S. K. Majee and A. Raychaudhuri, Nucl. Phys. B **760** (2007) 117 [arXiv:hep-ph/0608208]; P. Bandyopadhyay, B. Bhattacharjee and A. Datta, [arXiv:0909.3108 [hep-ph]]; B. Bhattacharjee, A. Kundu, S. K. Rai and S. Raychaudhuri, [arXiv:0910.4082 [hep-ph]]; B. Bhattacharjee and K. Ghosh, Phys. Rev. D **83** (2011) 034003 [arXiv:1006.3043 [hep-ph]].
- [29] A. Datta and S. Raychaudhuri, Phys. Rev. D **87** (2013) 035018 [arXiv:1207.0476 [hep-ph]]; U. K. Dey and T. S. Ray, arXiv:1305.1016 [hep-ph]; K. Nishiwaki, et al.[arXiv:1305.1686 [hep-ph]] [arXiv:1305.1874 [hep-ph]]; G. Bélanger, A. Belyaev, M. Brown, M. Kazikazi, and A. Pukhov, [arXiv:1207.0798 [hep-ph]]; A. Belyaev, M. Brown, J. M. Moreno, C. Papineau, [arXiv:1212.4858 [hep-ph]].
- [30] G. Bhattacharyya, P. Dey, A. Kundu and A. Raychaudhuri, Phys. Lett. B **628**, 141 (2005) [arXiv:hep-ph/0502031]; B. Bhattacharjee and A. Kundu, Phys. Lett. B **627**, 137 (2005) [arXiv:hep-ph/0508170]; A. Datta and S. K. Rai, Int. J. Mod. Phys. A **23**, 519 (2008) [arXiv:hep-ph/0509277]; B. Bhattacharjee, A. Kundu, S. K. Rai and S. Raychaudhuri, Phys. Rev. D **78**, 115005 (2008) [arXiv:0805.3619 [hep-ph]]; B. Bhattacharjee, Phys. Rev. D **79**, 016006 (2009) [arXiv:0810.4441 [hep-ph]].
- [31] T. Flacke, K. Kong and S. C. Park, arXiv:1303.0872 [hep-ph].
- [32] G. R. Dvali, G. Gabadadze, M. Kolanovic and F. Nitti, Phys. Rev. D **64** (2001) 084004 [arXiv:hep-ph/0102216].
- [33] M. S. Carena, T. M. P. Tait and C. E. M. Wagner, Acta Phys. Polon. B **33** (2002) 2355 [arXiv:hep-ph/0207056].
- [34] F. del Aguila, M. Perez-Victoria and J. Santiago, JHEP **0302** (2003) 051 [hep-th/0302023]; hep-ph/0305119.
- [35] F. del Aguila, M. Perez-Victoria and J. Santiago, Acta Phys. Polon. B **34** (2003) 5511 [hep-ph/0310353].
- [36] T. Flacke, A. Menon and D. J. Phalen, Phys. Rev. D **79** (2009) 056009 [arXiv:0811.1598 [hep-ph]].
- [37] For a discussion of BLKT in extra-dimensional QCD, see A. Datta, K. Nishiwaki and S. Niyogi, JHEP **1211** (2012) 154 arXiv:1206.3987 [hep-ph].

- [38] A. Datta, U. K. Dey, A. Shaw and A. Raychaudhuri, Phys. Rev. D **87** (2013) 076002 [arXiv:1205.4334 [hep-ph]].
- [39] C. Schwinn, Phys. Rev. D **69** (2004) 116005 [arXiv:hep-ph/0402118].
- [40] G. Belanger, M. Kakizaki and A. Pukhov, arXiv:1012.2577[hep-ph].
- [41] J. Bonnevier, H. Melbeus, A. Merle and T. Ohlsson, arXiv:1104.1430[hep-ph].
- [42] XENON Collaboration, Phys. Rev. Lett. **109** (2012) 181301; [arXiv:1301.6620[astro-ph.CO]]
- [43] G. Servant and T.M.P. Tait, New J. Phys. **4** (2002) 99 [arXiv: hep-ph/0209262].
- [44] H.-C. Cheng, J.L. Feng, and K.T. Matchev, Phys. Rev. Lett. **89** (2002) 211301 [arXiv: hep-ph/0207125].
- [45] S. Arrenberg, L. Baudis, K. Kong, K. T. Matchev and J. Yoo, Phys. Rev. D **78** (2008) 056002 [arXiv:0805.4210 [hep-ph]].